

SHEP-03-07  
 TSL/ISV-2003-0271  
 August 2003

# Pair production of charged Higgs bosons in association with bottom quark pairs at the Large Hadron Collider

S. Moretti<sup>1</sup>

School of Physics & Astronomy, University of Southampton,  
 Highfield, Southampton SO17 1BJ, UK

J. Rathsmann<sup>2</sup>

High Energy Physics, Uppsala University, Box 535, 751 21 Uppsala, Sweden

## Abstract

We study the process  $gg \rightarrow b\bar{b}H^\pm H^\mp$  at large  $\tan\beta$ , where it represents the dominant production mode of charged Higgs boson pairs in a Type II 2-Higgs Doublet Model, including the Minimal Supersymmetric Standard Model. The ability to select this signal would in principle enable the measurements of some triple-Higgs couplings, which in turn would help understanding the structure of the extended Higgs sector. We outline a selection procedure that should aid in disentangling the Higgs signal from the main irreducible background. This exploits a signature made up by 'four b-quark jets, two light-quark jets, a  $\tau$ -lepton and missing energy'. While, for  $\tan\beta > 30$  and over a significant  $M_H$  range above the top mass, a small signal emerges already at the Large Hadron Collider after  $100 \text{ fb}^{-1}$ , ten times as much luminosity would be needed to perform accurate measurements of Higgs parameters in the above  $\tan\beta$  state, rendering this channel a primary candidate to benefit from the so-called 'Super' Large Hadron Collider option, for which a tenfold increase in instantaneous luminosity is currently being considered.

## Keywords:

Beyond Standard Model, Two Higgs Doublet Models, Supersymmetry, Charged Higgs Bosons.

---

<sup>1</sup> stefano@hep.phys.soton.ac.uk

<sup>2</sup> johan.rathsmann@tsl.uu.se

# 1 Introduction

Charged Higgs bosons appear in the particle spectrum of a general 2-Higgs Doublet Model (2HDM). We are concerned here with the case of a Type II 2HDM [1], possibly in presence of minimal Supersymmetry (SUSY), the combination of the two yielding the so-called Minimal Supersymmetric Standard Model (MSSM). To stay with the Higgs sector of the extended model, unless two or more neutral Higgs states<sup>3</sup> are detected at the Large Hadron Collider (LHC), only the discovery of a spinless charged Higgs state would unquestionably confirm the existence of new physics beyond the Standard Model (SM), since such a field has no SM counterpart. In the MSSM, e.g., if  $M_H \gg M_{A^0}; M_{H^0} \approx M_{h^0}$  and  $\tan\beta$  is below 10 or so, the only available Higgs state ( $h^0$ ) is degenerate with the one of the SM: this is the so-called 'decoupling scenario'<sup>4</sup>.

Not surprisingly then, a lot of effort has been made lately, from theorists and experimentalists alike, in clarifying the Higgs discovery potential of the LHC in the charged Higgs sector [2]. (This is particularly true within the MSSM scenario, where one could also exploit interactions between the Higgs and sparticle sectors [3] in order to extend the reach of charged Higgs bosons at the LHC, beyond the standard channels.) Results are now rather encouraging, as charged Higgs bosons could indeed provide the key to unveil the nature of Electro-Weak Symmetry Breaking (EWSB) over a large area in  $M_H$  and  $\tan\beta$ , as they may well be the next available Higgs boson states, other than the  $h^0$ , provided  $\tan\beta$  is rather large (above 10 or so). Once the  $H^\pm$  and  $h^0$  Higgs bosons will have been detected, the next step would be to determine their interactions with SM particles, among them selves and also with the other two neutral Higgs states,  $H^0$  and  $A^0$ . While the measurement of the former would have little to teach us as whether one is in presence of a general Type II 2HDM or indeed the MSSM, constraints on the latter two would certainly help to clarify the situation in this respect. In fact, triple-Higgs vertices enter directly the functional form of the extended Higgs potential and, once folded within a suitable Higgs production process, may lead to the measurement of fundamental terms of the extended model Lagrangian. As

---

<sup>3</sup>Of the initial eight parameters pertaining to a complex Higgs doublet, only five survive as real particles upon Electro-Weak Symmetry Breaking (EWSB), labeled as  $h^0; H^0, A^0$  (the first two are CP-even or 'scalars' whereas the third is CP-odd or 'pseudoscalar') and  $H^\pm$ , as three degrees of freedom are absorbed into the definition of the longitudinal polarisation for the gauge bosons  $Z^0$  and  $W^\pm$ , upon their mass generation after EWSB.

<sup>4</sup>One of the Higgs masses, usually  $M_{A^0}$  or  $M_H$ , and the ratio of the Vacuum Expectation Values (VEVs) of the up-type and down-type Higgs doublets (denoted by  $\tan\beta$ ) are the two parameters that uniquely define the MSSM Higgs sector at tree-level.

the  $H^\pm$  states have a finite Electro-Magnetic (EM) charge, the first Lagrangian term of relevance would be the one involving two such states and a neutral Higgs boson: chiefy, the vertices  $H^\pm H^0 A^0$ , where  $A^0 = h^0$  and  $H^0$ .<sup>5</sup> This requires the investigation of hard scattering processes with two charged Higgs bosons in the final state, as their direct couplings to valence quarks in the proton would be very small, hence inhibiting processes like: e.g.,  $qq \rightarrow H^\pm H^\pm A^0$ .

## 2 Hadroproduction of charged Higgs boson pairs

A summary of all possible production modes of charged Higgs boson pairs at the LHC in the MSSM can be found in Ref. [4]. Three channels dominate  $H^\pm H^\pm$  phenomenology at the LHC: (i)  $qq \rightarrow H^\pm H^\pm$  (via intermediate  $Z^0$  production but also via Higgsstrahlung of incoming  $bb$  pairs) [5]; (ii)  $gg \rightarrow H^\pm H^\pm$  (primarily via a loop of top and bottom (s)quarks) [6]; (iii)  $qq \rightarrow qqH^\pm H^\pm$  (via vector boson fusion) [4]. Corresponding cross sections are found in Fig. 2 of Ref. [4]. For all phenomenologically relevant  $\tan\beta$  values it is essentially the first process which dominates. One important aspect should be noted here though, concerning the simulation of the  $bb$  component of the  $qq \rightarrow H^\pm H^\pm$  process, which can become the dominant contribution to the cross section of process (i) at very large  $\tan\beta$  values. In fact, the use of a 'phenomenological' b-quark parton density, as available in most Parton Distribution Function (PDF) sets currently on the market, requires crude approximations of the partonic kinematics, which result in a mis-estimation of the corresponding contribution to the total production cross section. (The problem is well known already from the study of the leading production processes of charged Higgs bosons at the LHC, namely,  $bg \rightarrow tH^\pm$  and  $gg \rightarrow bH^\pm$ : see, e.g., [8, 10].) In practice, the b-(anti)quark in the initial state comes from a gluon in the proton beam splitting into a collinear  $bb$ -pair, resulting in large factors of  $\frac{1}{s} \log(\frac{\mu_F}{m_b})$ , where  $\mu_F$  is the factorisation scale. These terms are then re-summed to all orders,  $\sum_n \frac{1}{s} \log^n(\frac{\mu_F}{m_b})$ , in evaluating the phenomenological b-quark PDF. In contrast, in using a gluon density while computing the 'tw in' process (iv)  $gg \rightarrow bbH^\pm H^\pm$  (see Fig. 1 for the associated Feynman graphs), one basically only includes the first terms ( $n = 1$ ) of the corresponding two series, when the b and  $\bar{b}$  in the final state are produced collinearly to the incoming gluon directions. It turns out that, for  $\mu_F \sim m_b$ , as it is the case here if one uses the standard choice of factorisation

---

<sup>5</sup>We are here only considering CP-conserving extensions of the SM Higgs sector such that there is no  $\langle H^\pm H A^0 \rangle$ -vertex".

scale  $\mu_F > 2M_H$ , the re-summed terms are large and over-compensate the contribution of the large transverse momentum region available in the gluon-induced case. In the end, differences between the two cross sections as large as one order of magnitude are found, well in line with the findings of Refs. [8] and [10], if one considers that two  $g \rightarrow b\bar{b}$  splittings are involved here.

One way to reconcile the large differences in the cross section for the two processes,  $gg \rightarrow b\bar{b}H^+H^-$  and  $b\bar{b} \rightarrow H^+H^-$ , is to use a significantly lower factorisation scale, as argued in [11, 12, 13] for similar processes. Following the suggestion in part A.1. of [14], we look at the transverse momentum distribution of the b-quarks in the process  $gg \rightarrow b\bar{b}H^+H^-$ , as shown in Fig. 2, to get an indication of the most suitable factorisation scale for  $b\bar{b} \rightarrow H^+H^-$ . From the figure we see that a proper choice for the latter, when  $M_H = 215$  GeV, is of the order  $\mu_F = 0.1 \sqrt{s} \approx 40$  GeV (at this point the distribution reaches about half of its "plateau" value<sup>6</sup>) rather than, e.g.,  $\mu_F = \sqrt{s}$ . Using such a lower scale we do get a much better agreement between the leading order (LO) cross sections for the two processes, as shown in Tab. 1 in the case of the MSSM specified below ( $M_{A^0} = 200$  GeV and  $\tan\beta = 30$ ) if the renormalisation scale ( $\mu_R$ ) is also changed accordingly. However, one should also bear in mind that both processes are subject to possibly large QCD corrections and that the choice of (factorisation and/or renormalisation) scales that minimises the differences between the two descriptions in higher orders of  $H^+H^-$  production may alternatively be viewed as the most suitable one. Or else, one may arguably choose a scale that minimises the size of the higher order corrections themselves in either process independently of the other. All such additional values may eventually turn out to be different from the one extracted from Tab. 1. Such exercises in higher orders cannot unfortunately be performed in the present context, as next-to-leading order (NLO) corrections to the two processes of interest are unavailable. Yet, some guidance may be afforded again by the study of the single charged Higgs production modes already referred to. In fact, NLO corrections to  $bg \rightarrow tH^+$  were first computed in Ref. [7] and then later confirmed in [11]. Following Ref. [11], it is clear that a choice for the renormalisation scale  $\mu_R$  as low as the one recommended for the factorisation one  $\mu_F$  is not sustainable for  $bg \rightarrow tH^+$  at NLO, no matter the choice for the latter: see Fig. 5 of [11]. Besides, if one fixes, e.g.,  $\mu_R = (m_t + M_H) = 2$  but varies  $\mu_F$ , the minimal difference between the NLO and the LO results for  $bg \rightarrow tH^+$  is found at large  $\mu_F$ , at values around or even larger than  $m_t + M_H$  (again, see Fig. 5 of Ref. [11]). Be the most

---

<sup>6</sup>This number is not too dissimilar from the one recommended in [12] on the basis of the same argument applied to the single Higgs production mode  $gg \rightarrow b\bar{b}H^+$ , as  $M = 4$ , where  $M$  is the threshold mass  $m_t + M_H$ .

Table 1: Cross sections for  $gg \rightarrow bbH^+H^-$  and  $bb \rightarrow H^+H^-$  as functions of the factorisation ( $\mu_F$ ) and renormalisation ( $\mu_R$ ) scales (at leading order the  $bb \rightarrow H^+H^-$  cross section does not depend on  $\mu_R$ ) in the MSSM specified below ( $M_{A^0} = 200$  GeV and  $\tan\beta = 30$ ).

$\mu_F$	$\mu_R$	$(gg \rightarrow bbH^+H^-)$ [fb]	$(bb \rightarrow H^+H^-)$ [fb]
$\mu_F = \mu_R$	$\mu_R$	1.4	
$hm_b^T i^Y$	$\mu_R$	2.3	
$hm_b^T i^Y$	$hm_b^T i^Y$	8.2	
$\mu_F = \mu_R$			7.5
$\mu_F = \mu_R$			4.4

<sup>y</sup> Here, the exact definition is:  $hm_b^T i = \frac{q}{m_b^2 + ((p_b^T)^2 + (p_b^T)^2)} = 2$ .

suitable combination of scales as it may, we take here a pragmatical attitude and use the standard setup  $\mu_F = \mu_R = \mu$  throughout, as this corresponds to the most conservative choice in terms of the overall normalisation for  $gg \rightarrow bbH^+$  (Tab.1) (as it becomes minimal) and keeping in mind that its cross section can be up to a factor 5 larger depending on the choice of factorisation and renormalisation scales.

Under any circumstances, a clear message that emerged from NLO computations of  $bg \rightarrow tH^+$  with respect to the LO ones of  $gg \rightarrow bbH^+$  is that the former (duly incorporating a running NLO b-quark mass in the Yukawa coupling to the charged Higgs boson) agree better with the latter if these use the pole b-quark mass instead, see Fig. 4 of Ref. [11]. By analogy, in the remainder of our paper, we will make the same assumption (of a pole b-quark mass entering the  $btH^+$  vertex) in our  $gg \rightarrow bbH^+H^-$  process at LO. Finally, while a well defined procedure exists in order to compute both inclusive and exclusive cross sections when combining the bb- and gg-initiated processes, through the subtraction of the common logarithmic terms [8] and/or by a cut in phase space [9], it should be noticed that process (iv) is the only contributor when one exploits the tagging of both the two b-quark jets produced in association with the charged Higgs boson pair.

It is precisely the intention of this note that of pursuing a similar strategy in order to extract a possible  $bbH^+H^-$  signal, as it has already been shown the beneficial effects of triggering on the 'spectator' b-jet in the  $gg \rightarrow t\bar{t}H$  case, in order to improve on the discovery reach of charged Higgs bosons at the LHC [15]. Furthermore, if vertices of the type  $H^+H^0$  are to be studied experimentally, one should appreciate the importance of the  $gg \rightarrow bb^0$  subprocess (from which two charged Higgs bosons would stem out of the above triple-Higgs

coupling: see diagrams 4;8;14;19;23;29;34 and 38 in Fig. 1) by recalling that the latter reaction is the dominant production mode of neutral Higgs scalars (chiefly, the  $H^0$  state) at  $\tan\beta$  values above 7 or so, for any neutral Higgs mass of phenomenological interest [16], this justifying our choice of privileging here the  $gg \rightarrow b\bar{b}H^+H^-$  channel. Finally, whereas the already recalled MSSM relation  $M_{H^\pm} = M_{A^0} = M_{H^0} = M_{h^0}$  clearly prevents the appearance of a  $H^0 \rightarrow H^+H^-$  resonance in the diagrams proceeding via intermediate states of the form  $gg \rightarrow b\bar{b}H^0$ , this is no longer true in a general 2HDM, wherein one may well have  $M_{H^0} > 2M_{H^\pm}$ , with the consequent relative enhancement of this subset of diagrams with respect to all others appearing in Fig. 1.

We will attempt the signal selection for the case of rather heavy charged Higgs bosons, with masses above that of the top quark. The case for the existence of such massive Higgs states has in fact become phenomenologically pressing, since rumours of a possible evidence of light charged Higgs bosons being produced at LEP2 [17] have faded away. Instead, one is now left from LEP2 with a model independent limit on  $M_{H^\pm}$ , of order  $M_W$ . Within the MSSM, the current lower bound on a light Higgs boson state, of approximately 110 GeV [18], can be converted at two-loops into a minimal value for the charged Higgs boson mass, of order 130{140 GeV, for  $\tan\beta \leq 3$ {4<sup>7</sup>. This bound grows rapidly stronger as  $\tan\beta$  is decreased while tapering very gradually as  $\tan\beta$  is increased (staying in the 110{125 GeV interval for  $\tan\beta > 7$ ). Besides, in the mass interval  $M_{H^\pm} < m_t$ , charged Higgs bosons could well be found at Tevatron (Run 2) [20], which has already begun data taking at  $\sqrt{s_{pp}} = 2$  TeV at FNAL, by exploiting their production in top decays,  $t \rightarrow bH^+$ , and the tau-neutrino detection mode,  $H^+ \rightarrow \tau\nu$ . In contrast, if  $M_{H^\pm} > m_t$  (our definition of a heavy charged Higgs boson), one will necessarily have to wait for the advent of the LHC,  $\sqrt{s_{pp}} = 14$  TeV, at CERN. As hinted at in the beginning, we also make the assumption in our study that the charged Higgs boson mass is already known, e.g., from studies of the leading production and decay channels,  $gg \rightarrow t\bar{t}H^\pm$  and  $H^\pm \rightarrow t\bar{b}$  or  $b\bar{t}$ , during the first years of running of the CERN hadron machine.

Under the above parameter assumptions, i.e., large  $\tan\beta$  ( $> 10$ ) and large  $M_{H^\pm}$  values ( $> m_t$ ), a sensible choice of decay channels [21] for our pair of charged Higgs bosons would be to require one to decay via the leading mode, i.e.,  $H^+ \rightarrow t\bar{b}$  (with the t-quark further decaying hadronically, so to allow for the kinematic reconstruction of the charged Higgs boson resonance in a four-jet system) and the other via  $H^- \rightarrow b\bar{t}$  (whose rate

---

<sup>7</sup>Recall that the tree-level relation between the masses of the charged and pseudoscalar Higgs boson,  $M_{H^\pm}^2 = M_{A^0}^2 + M_W^2$ , is almost invariably quite insensitive to higher order corrections [19].

increases with  $\tan\beta$  and that yields a somewhat cleaner trigger in the LHC environment, independently of whether the  $\tau$ -lepton decays leptonically or hadronically, as opposed to the above multi-jet and high hadron-multiplicity signature). As such decays would induce an intermediate signal state made up by  $b\bar{b}b$  and since we will assume tagging all four  $b$ 's, it is clear that the dominant irreducible background would be  $b\bar{b}t$  production followed by the decay  $t \rightarrow bW \rightarrow b$ .

### 3 Calculation

The hard subprocess describing our signal is then

$$gg \rightarrow b\bar{b}H^+H^-; \quad (1)$$

whereas for the main irreducible background we have to deal with

$$gg \rightarrow b\bar{b}t; \quad (2)$$

(We neglect here the computation of the quark-antiquark initiated components of both signal and background, i.e.,  $q\bar{q} \rightarrow b\bar{b}H^+H^-$  and  $q\bar{q} \rightarrow b\bar{b}t$ , respectively, as they are negligible at the LHC, in comparison to the gluon-gluon induced modes.) The matrix elements for (1)–(2) have been calculated by using the HELAS [22] subroutines and MadGraph [23]. All unstable particles entering the two processes ( $t; H^\pm$  and  $W^\pm$ ) were generated not only on-shell (i.e., with their natural widths) but also in Narrow Width Approximation (NWA) for comparison. For the MSSM and 2HDM Higgs bosons, the program HDECAY [24] has been exploited to generate the decay rates eventually used in the Monte Carlo (MC) simulations. For the MSSM, we have assumed the following set up for the relevant SUSY input parameters:  $\mu = 0$ ,  $A_\nu = A_u = A_d = 0$  (with  $\nu = e; \tau$ ; and  $u=d$  referring to  $u=d$ -type quarks) and  $M_{\text{SUSY}} = 1 \text{ TeV}$ , the latter implying a sufficiently heavy scale for all sparticle masses, so that no  $H^\pm \rightarrow \text{SUSY}$  decay can take place<sup>8</sup>.

As a 2HDM configuration, we have basically maintained the previous setup in the relevant input parameters of HDECAY, with the most important difference being the assumption of a different relation between the input  $M_{A^0}$  value and the derived  $M_{H^0}$  one, by assuming a linear relation between the  $H^0$  and  $A^0$  masses, i.e.,  $M_{H^0} = x M_{A^0}$ , with  $x$  being a number

<sup>8</sup>The only possible exception in this mass hierarchy would be the Lightest Supersymmetric Particle (LSP), whose mass may well be smaller than the  $M_H$  values that we will be considering, a state in which however a charged Higgs boson cannot decay to, as R-parity and EM charge conservation would require the presence of an additional heavy chargino.

larger than 2, while maintaining the MSSM relations among the  $h^0; H^0$  and  $A^0$  masses, thereby allowing for the already intimated onset of  $H^0 \rightarrow H^+ H^-$  resonant decays in diagrams 4;8;14;19;23;29;34 and 38 of Fig. 1. As already remarked upon, this is a crucial phenomenological difference with respect to the MSSM, wherein such a decay threshold is never reached over the unexcluded region of parameter space. Another important difference in a more general 2HDM is the value of the triple Higgs coupling  $g_{H^0 H^+ H^-}$  which is not necessarily the same as in the MSSM.

Before giving the details of the 2HDM setup we are using let us recall the most general CP-conserving 2HDM scalar potential which is symmetric under  $U(1) \times U(1)$  up to softly breaking dimension-2 terms (thereby allowing for loop-induced flavour changing neutral currents) [1],

$$\begin{aligned}
 V(\varphi_1; \varphi_2) = & \frac{1}{2} \left( \frac{y_1}{h} \varphi_1 - \frac{v_1}{\sqrt{2}} \right)^2 + \frac{2}{2} \left( \frac{y_2}{h} \varphi_2 - \frac{v_2}{\sqrt{2}} \right)^2 \\
 & + \frac{3}{2} \left( \frac{y_1}{h} \varphi_1 - \frac{v_1}{\sqrt{2}} \right) \left( \frac{y_2}{h} \varphi_2 - \frac{v_2}{\sqrt{2}} \right) \\
 & + \frac{4}{2} \left( \frac{y_1}{h} \varphi_1 \right) \left( \frac{y_2}{h} \varphi_2 \right) + \frac{5}{2} \text{Re} \left( \frac{y_1}{h} \varphi_1 \right) \left( \frac{y_2}{h} \varphi_2 \right) + \frac{6}{2} \text{Im} \left( \frac{y_1}{h} \varphi_1 \right) \text{Im} \left( \frac{y_2}{h} \varphi_2 \right)
 \end{aligned} \quad (3)$$

where  $v_1^2 + v_2^2 = v^2 = 2M_W^2/g^2 \approx (174 \text{ GeV})^2$ . In general, the potential is thus parameterised by seven parameters (the  $v_i$  and  $\tan \beta = v_2/v_1$ ) whereas in the MSSM only two of them are independent. In the following we will replace  $v_i$  with the masses of the Higgs bosons ( $M_{h^0}; M_{H^0}; M_{A^0}; M_{H^\pm}$ ) and the mixing angle of the CP-even Higgs bosons.

From the scalar potential the different three- and four-Higgs couplings can be obtained. (See [25, 26] for a complete compilation of couplings in a general CP-conserving 2HDM.) Using the Higgs masses and  $\tan \beta$  as parameters together with  $\lambda_3$  the  $g_{H^0 H^+ H^-}$  coupling takes a particularly simple form (see for example [27])

$$\begin{aligned}
 g_{H^0 H^+ H^-} = & \frac{g}{M_W} \cos(\alpha - \beta) M_{H^\pm}^2 - \frac{M_{H^0}^2}{2} + \frac{\sin(\alpha + \beta)}{\sin 2\beta} \frac{1}{2} (M_{H^0}^2 + M_{h^0}^2) + \\
 & + 4 \lambda_3 v^2 \frac{1}{2 \sin 2\beta} [\sin 2\beta + 2 \sin(\alpha - \beta) \cos(\alpha + \beta)] (M_{H^0}^2 - M_{h^0}^2) \quad : (4)
 \end{aligned}$$

For the other three- and four-Higgs couplings we refer to [25, 26].

In the 2HDM that we will adopt below we will start from the MSSM parameter values for  $M_{H^0}; M_{A^0}; M_{h^0}; M_{H^\pm}; \tan \beta; \lambda_3; \lambda_4; \lambda_5; \lambda_6; \lambda_7; \lambda_8; \lambda_9; \lambda_{10}$  using  $M_{A^0}$  and  $\tan \beta$  as input. As already mentioned we then change from  $M_{H^0}^{\text{MSSM}}$  to  $M_{H^0}^{2\text{HDM}} = 2.5 M_{A^0}$  such that  $M_{H^0} > 2 M_{H^\pm}$  while keeping all the other Higgs boson masses and  $\tan \beta$  fixed. The remaining two parameters,

Table 2: Examples of values of the parameters in the Higgs potential used for different values of  $M_{A^0}$  together with the corresponding values of  $\beta$  and  $g_{H^0H^+H^-}$ .

$M_{A^0}$ [GeV]	1	2	3	4	5	6	$g_{H^0H^+H^-}$ [GeV]	
150	6.660	7.370	7.557	0.9419	4.263	0.7454	0.2857	1307
200	7.653	10.74	10.94	1.522	7.814	1.325	0.2258	1532
250	3.407	12.33	12.52	2.267	12.53	2.071	0.1696	1305
300	1.150	.6957	5.352	3.178	0.4246	2.982	1.531	3410
350	11.81	0.7778	5.565	4.255	0.3598	4.058	1.541	3786
400	8.421	1.574	6.711	5.497	0.3722	5.301	1.543	4653

and  $(\beta_5, \beta_6)=2$ , are then determined by randomly picking one million  $(\beta_5, \beta_6)=2$ -points, in the ranges  $[\beta_5 = -2; \beta_5 = 2]$  and  $[\beta_6 = -4; \beta_6 = 4]$  respectively, and keeping the one which gives the largest effective coupling,  $g_{H^0H^+H^-} \cos \beta$ , thereby also taking into account the  $H^0bb$ -coupling. In order to accept a point we also check that the following conditions are fulfilled: the potential is bounded from below, the  $\beta_i$  are kept small enough ( $|\beta_i| < 4$ ) to remain in the perturbative regime, the contribution to  $\Omega_{CDM}$   $< 10^{-3}$  (although with the above setup for the Higgs masses we are more or less guaranteed not to violate any experimental bounds on the  $\beta$ -parameter [1]), and the combined partial width for the three  $H^0 \rightarrow h^0h^0; A^0A^0; H^+H^-$  decays is smaller than  $M_{H^0}=2$ . (We have checked that the partial widths of the  $H^0 \rightarrow h^0h^0h^0; h^0A^0A^0; h^0H^+H^-$  decay channels are negligible.)

Some examples of the actual values of the  $\beta_i$  we use in this study are given in Tab. 2<sup>9</sup> together with the corresponding values of  $\beta$  and  $g_{H^0H^+H^-}$ . From the table one sees that for  $M_{A^0} > 300$  GeV the preferred solution is quite different from the one for  $M_{A^0} < 250$  GeV. This will be even more clear below when looking at the cross section as a function of  $M_{H^0}$ , but already now the large value of  $\beta$  is hinting at the fact that the cross section will be much smaller for  $M_{A^0} > 300$  GeV since the  $H^0bb$ -coupling is proportional to  $\cos \beta$ . However, it should be kept in mind that the 2HDM setup we are using is not the most general one based on the scalar potential (3) and that there are certainly other parts of the parameter space which we have not scanned that give a larger cross section (for example by letting the mass of the lightest CP-even Higgs  $M_{h^0}$  being a free parameter).

<sup>9</sup>The selection procedure outlined above did not lead to any acceptable solution for  $M_{A^0} > 580$  GeV.

To get an explicit example of the large differences between the more general 2HDM we are considering and the MSSM, we compare the two using  $M_{A^0} = 200 \text{ GeV}$  and  $\tan\beta = 30$  as input values, as we will do below. In this case we get  $g_{H^0 H^+ H}^{2\text{HDM}} = 1532 \text{ GeV}$  in the 2HDM instead of the MSSM value,  $g_{H^0 H^+ H}^{\text{MSSM}} = 1.8 \text{ GeV}$ . With the value of  $\kappa^{2\text{HDM}} = 0.2258$  not being much larger than  $\kappa^{\text{MSSM}} = 0.05774$  the difference in effective coupling  $g_{H^0 H^+ H} \cos\alpha$  is close to a factor one thousand and as we will see below it has a large impact on the magnitude of the cross section. (The  $H^0$  widths will of course be different too in the MSSM and 2HDM just described: their effects have been included in the numerical analysis.)

As intimated already in Sect. 2, a non-running b-quark mass was adopted for both the kinematics and the Yukawa couplings:  $m_b = 4.25 \text{ GeV}$ . For the top parameters, we have taken  $m_t = 175 \text{ GeV}$  with  $\alpha_t$  computed according to the model used (in the limit  $M_H \gg m_t$ , we have  $\alpha_t = 1.56 \text{ GeV}$  in both the 2HDM and MSSM scenarios considered here). EW parameters were as follows:  $\alpha_{EM} = 1/128$ ,  $\sin^2\theta_W = 0.232$ , with  $M_{Z^0} = 91.19 \text{ GeV}$  ( $M_{Z^0} = 2.50 \text{ GeV}$ ) and  $M_W = M_{Z^0} \cos\theta_W$  ( $M_W = 2.08 \text{ GeV}$ ). For the  $\tau$ -lepton mass we used  $m_\tau = 1.78 \text{ GeV}$ , whereas all the other leptons and quarks were assumed to be massless.

The integrations over the multi-body final states have been performed numerically with the aid of VEGAS [28], Metropolis [29] and RAMBO [30], for checking purposes. Finite calorimeter resolution has been emulated through a Gaussian smearing in transverse momentum,  $p_{q\perp}^T$ , with  $(p_{q\perp}^T)_{\text{smear}}^2 = (0.60 p_{q\perp}^T)^2 + (0.04)^2$  for all jets and  $(p_{q\perp}^T)_{\text{smear}}^2 = (0.12 p_{q\perp}^T)^2 + (0.01)^2$  for leptons. The corresponding missing transverse momentum,  $p_{\text{miss}}^T$ , was reconstructed from the vector sum of the visible momenta after resolution smearing. Furthermore, we have identified jets with the partons from which they originate and applied all cuts directly to the latter, since parton shower and hadronisation were not included in our study. In addition the  $\tau$ -lepton decays have not been considered except where specially stated.

As default PDFs we have adopted the set MR S98LO (05A) [31] with  $Q = \sqrt{s}$  as factorisation/renormalisation scale for both signal and background. The same scale entered the evolution of  $\alpha_s$ , which was performed at one-loop, with a choice of  $n_f = 4$  consistent with the PDF set adopted. In fact, we have verified that the spread in the inclusive cross sections, for both signal and background, as obtained by using the five different parameterisations of MR S98LO and also CTEQ 4L [31] was within 6–7% of the values quoted for MR S98LO (05A) in the remainder of the paper.

## 4 Selection

The signature that we are then considering is in practice:

$$4 \text{ b-jets} + 2 \text{ light-jets} + \text{ } + p_{\text{miss}}^T; \quad (5)$$

wherein the two b-jets from the hard process are actually defined as the two most forward/backward ones that also display a displaced vertex.

We have assumed a conservative (optimistic) detector configuration by imposing acceptance and separation cuts on all light-quark (including c's) and b-jets, labeled as j and b, respectively, as follows:

$$p_b^T > 10 (20) \text{ GeV}; \quad |j_b| < 2.5 (5); \quad p_j^T > 20 \text{ GeV}; \quad |j_j| < 5; \quad R_{jj;jb} > 0.4: \quad (6)$$

The two most forward/backward b-jets (with pseudorapidities of opposite sign) are further required to yield

$$M_{bb} > M_H \quad (7)$$

for their invariant mass. For leptons (independently of whether they are decayed or not) we impose:

$$p^T > 10 \text{ GeV}; \quad |j_j| < 2.5 (5); \quad R_{j;lb} > 0.4: \quad (8)$$

The conservative setup corresponds to the standard ATLAS/CMS detectors whereas the optimistic one may be viewed as the upgrade foreseen for the same apparatus in the context of the Super LHC (SLHC) option [32]<sup>10</sup>.

Having now excluded the two b-jets fulfilling eq. (7) from the list of jets, we impose hadronic W- and t-mass reconstruction:

$$M_{jj} - M_W - |j| < 15 \text{ GeV}; \quad M_{bjj} - m_t < 35 \text{ GeV}; \quad (9)$$

where the two light-quark jets entering the last inequality are of course the same fulfilling the first one. Finally, the missing transverse momentum should be:

$$p_{\text{miss}}^T > M_H = 4: \quad (10)$$

---

<sup>10</sup> If the required b-tagging at transverse momenta of 10 GeV (yet within 2.5 in pseudorapidity) may well be achieved with high efficiency by the two mentioned LHC collaborations, see [33], especially if the two forward/backward 'jets' are not required to be identified as such, rather as collimated hadronic activity displacing a secondary vertex, this can no longer be the case at the SLHC, for which we have then assumed a 20 GeV threshold.

The combined effects of these cuts on the signal (1) in the MSSM and 2HDM models is shown in Figs. 3 and 4 respectively in the case of retaining the finite width effects using on-shell masses for the  $H$  and  $W$ . (The difference when instead using the NWA is very small and this option is therefore not shown.) As can be seen from the figures the effects of the cuts on the magnitude of the cross sections is quite severe. On the other hand the cuts are needed (especially in case of the MSSM) in order to beat down the background as is illustrated in Fig. 5 for the two different detector options. From the figure it is also clear that the signal cross section reaches its maximum around  $M_H = 200$  GeV and that the magnitude of the signal varies by up to 2 orders of magnitude depending on which model we are considering. It should also be noted that in the 2HDM setup we are using it does not make much sense to go above  $M_H \lesssim 400$  GeV (corresponding to  $M_{H^0} = 1000$  GeV) since in this case the width of the heavy neutral Higgs boson becomes comparable to its mass. In the following we will be considering the case  $M_H \lesssim 215$  GeV (corresponding to  $M_{A^0} = 200$  GeV) in more detail.

After the above cuts have been implemented and the jet momenta assigned, one can reconstruct the would-be charged Higgs boson mass, by pairing the three jets entering the equation in the right-hand side of (9) with the left-over central jet, a quantity which we denote by  $M_{4\text{jets}}$ . The corresponding mass spectrum is presented in Fig. 6 for our two customary setups of MSSM and 2HDM, assuming  $M_H = 215$  GeV and  $\tan\beta = 30$  as representative values. The figure shows clear peaks at the charged Higgs boson mass for the signal on top of a combinatorial background in both models whereas for the background process there is no such peak. Thus, by selecting events with

$$180 \text{ GeV} < M_{4\text{jets}} < 250 \text{ GeV} \quad (11)$$

we can get an additional discrimination against the background.

Furthermore, using the visible lepton momentum and the missing transverse one, it is possible to reconstruct the transverse mass, as

$$M^T = \sqrt{2p_{\text{miss}}^T (1 - \cos\theta)}; \quad (12)$$

with  $\theta$  the relative angle between the two momenta, a quantity which is ultimately correlated to the actual value of the mass resonance yielding  $H$  pairs ( $H$  in the signal and  $W$  in the background). We show this observable in Fig. 7 (where it is denoted by  $M_T$ ), again, for our two customary setups of MSSM and 2HDM. From the figure it is clear that the transverse mass for the signal in the two models extends all the way out to  $M_H$ .

Comparing with the background, which drops drastically around  $M^{\pm} = M_W$ , we see that it is advantageous to introduce a cut on the transverse mass of the order of

$$M^{\pm} > M_H = 2 \quad (107 \text{ GeV}) : \quad (13)$$

After having reconstructed the two charged Higgs bosons and applied the respective cuts (11) and (13) we can form the (effective, transverse) mass  $M_{4\text{jets}^{\pm}}$  of the combined two charged Higgs boson system, giving the possibility to look for possible resonances. As can be seen from the magnitudes of the cross sections in Fig. 8 the selection outlined above gives a very clear signal, although very small in the MSSM case, with essentially no background. From the figure it is also clear that there is a significant difference in shape between the two models, but it is not clear to what extent this can be used to extract any information about possible  $H^0 \rightarrow H^+ H^-$  resonances and the corresponding coupling based on shape only. (Notice the effects of finite detector resolution, emulated by our Gaussian smearing, that lead to  $M_{4\text{jets}^{\pm}}$  extending over a wide mass range both below and above  $2M_H$ .)

One possibility to get a more pronounced mass peak in the 2HDM case could be to use the kinematic constraint from the charged Higgs boson mass to reconstruct the longitudinal momentum of the  $\tau$  and then look at the actual invariant mass of the two charged Higgs bosons. In order to get a reasonable estimate of the possibilities of such a procedure we have also taken the decay of the  $\tau$ -lepton into account using the PYTHIA [34] MC event generator. However, even after the longitudinal momentum of the neutrinos from the  $H$  is reconstructed, there is no evident peak in the  $H^+ H^-$  invariant mass distribution (denoted by  $M(H^+ H^-)$ ) as illustrated in Fig. 9<sup>11</sup>. The reason for the disappearance of the peak is simply the smearing due to the detector resolution as is evident from Fig. 10. (For illustration, we have shown the results of the exercise for the case of the LHC cuts, although we have verified that the outcome is the same for the SLHC setup.)

## 5 Conclusion

As we have shown, it is possible to outline a selection procedure that enables one to extract a signal of heavy charged Higgs pair production in association with two b-quarks at  $\tan \beta > 30$  in extensions of the standard model with two Higgs doublets of Type II. In a general case the mass relations in the Higgs sector may be favourable such that a sizeable signal would

---

<sup>11</sup>When calculating the energy of the two neutrinos from the  $H$  it is assumed that their combined invariant mass vanishes.

appear already at the LHC through the resonant channel  $gg \rightarrow b\bar{b}H^0 \rightarrow b\bar{b}H^+H^-$ . However, in the MSSM the resonance is not accessible over the allowed parameter region and the non-resonant contributions turn out to be very small making it difficult to extract a signal even after upgrading the luminosity at LHC by a factor ten (SLHC). The large difference in cross section between the MSSM and a more general 2HDM shows that indeed the pair production of charged Higgs production is sensitive to the  $H^0H^+H^-$  coupling even though it will probably be difficult to reconstruct a resonant mass peak mainly due to the finite detector resolution.

In our study we have not included effects of the b-tagging efficiency. On the one hand, requiring four b-tags will give a sizeable reduction (of the order of a factor ten) of the signal as well as the backgrounds. On the other hand, the selection procedure outlined above was designed to get a clear signal in the case of the MSSM leading to unnecessarily tight cuts for the general 2HDM case. Furthermore, being a leading order calculation, the cross section we get for the signal is also sensitive to the choice of factorisation and renormalisation scales. If we, instead of using the standard choice of the invariant mass of the hard subsystem, use the mean transverse mass of the two b-quarks in the  $gg \rightarrow b\bar{b}H^+H^-$  process as scale, the cross section increases by a factor 5. Such a scale choice also gives a better agreement with the cross section for the 'tw in' process  $b\bar{b} \rightarrow H^+H^-$ . In order to get a better handle on the uncertainties due to scale choices a next-to-leading order calculation will eventually be necessary. Nonetheless, we believe that our results already call for the attention of ATLAS and CMS in further exploring the scope of the (S)LHC in reconstructing the form of the Higgs potential in extended models through signals of charged Higgs boson pairs.

## Acknowledgements

SM is grateful to The Royal Society of London (UK) for partial financial support in the form of a Study Visit and thanks the High Energy Theory Group of the Department of Radiation Science of Uppsala University for kind hospitality.

## References

- [1] J.F. Gunion, H.E. Haber, G.L. Kane and S. Dawson, "The Higgs Hunter's Guide" (Addison-Wesley, Reading MA, 1990), Erratum, hep-ph/9302272.

- [2] D A .D icus, J.L.Hewett, C .K ao and T G .R izzo, Phys.Rev.D 40, 787 (1989); J.F .G u-  
nion, Phys.Lett.B 322, 125 (1994); V .B arger, R J.N .P hillips and D P .R oy, Phys.  
Lett.B 324, 236 (1994); S.Raychaudhuri and D P .R oy, Phys.Rev.D 52, 1556 (1995),  
ibid.D 53, 4902 (1996); S.M oretti and K .O dagiri, Phys.Rev.D 55, 5627 (1997), ibid.  
D 59, 055008 (1999); D P .R oy, Phys.Lett.B 459, 607 (1999); S.M oretti and D P .R oy,  
Phys.Lett.B 470, 209 (1999); M .D rees, M .G uchait and D P .R oy, Phys.Lett.B 471,  
39 (1999); F .B orzum ati, J.-L.K neur and N .P olonsky, Phys.Rev.D 60, 115011 (1999);  
K .O dagiri, hep-ph/9901432; A A .B arrientos Bendezu and B A .K niehl, Phys.Rev.  
D 59, 015009 (1999), ibid.D 61, 097701 (2000), ibid.D 63, 015009 (2001); D J.M iller,  
S.M oretti, D P .R oy and W J .S tirling, Phys.Rev.D 61, 055011 (2000); S.M oretti,  
Phys.Lett.B 481, 49 (2000); O .B rein, W .H ollik and S .K anem ura, Phys.Rev.D  
63, 095001 (2001). For recent experimental studies and reviews, see: K A .A ssam agan,  
ATL{PHYS{99{013 and ATL{PHYS{99{025; K A .A ssam agan and Y .C oadou, ATL{  
COM {PHYS{2000{017; K A .A ssam agan et al, hep-ph/0002258; K A .A ssam agan,  
Y .C oadou and A .D eandrea, Eur.Phys.J.direct C 9, 1 (2002).
- [3] M .B isset, M .G uchait and S.M oretti, Eur.Phys.J.C 19, 143 (2001); K A .A ssam -  
agan, M .B isset, Y .C oadou, A K .D atta, A .D eandrea, A .D juadi, M .G uchait, Y .  
M am brini, F .M oortgat and S.M oretti, in hep-ph/0203056; S.M oretti, proceedings of  
the 'Seventh W orkshop on H igh Energy Physics Phenom enology W HEPP-V II', Harish  
Chandra Research Institute, Allahabad, India, 4-15 January 2002, hep-ph/0205104;  
A .D atta, A .D juadi, M .G uchait and F .M oortgat, hep-ph/0303095; M .B isset, F .  
M oortgat and S.M oretti, hep-ph/0303093; A .D atta, A .D juadi, M .G uchait and  
Y .M am brini, Phys.Rev.D 65, 015007 (2002); H .B aer, M .B isset, X .T ata and J .  
W oodside, Phys.Rev.D 46, 303 (1992).
- [4] S.M oretti, J.Phys.G 28, 2567 (2002).
- [5] E .E ichten, I.H inchli e, K .L ane and C .Q uigg, Rev.M od.Phys. 56, 579 (1984).
- [6] S.S.D .W illenbrock, Phys.Rev.D 35, 173 (1987); Y .Jiang, W .G .M a, L .H an, M .  
H an and Z .H .Yu, J.Phys.G 23, 385 (1997), Erratum , ibidem G 23, 1151 (1997);  
A .K rause, T .P lehn, M .S pira and P M .Z erwas, Nucl.Phys.B 519, 85 (1998); A .  
Belyaev, M .D rees, O J.P .Eboli, J.K .M izukoshi and S F .N ovaes, Phys.Rev.D 60,  
075008 (1999); A .Belyaev, M .D rees and J.K .M izukoshi, Eur.Phys.J.C 17, 337  
(2000); A A .B arrientos Bendezu and B A .K niehl, Nucl.Phys.B 568, 305 (2000); O .  
B rein and W .H ollik, Eur.Phys.J.C 13, 175 (2000).

- [7] S.H. Zhu, *Phys. Rev. D* 67, 075006 (2003).
- [8] F. Borzumati, J.-L. Kneur and N. Polonsky, in Ref. [2].
- [9] A. Belyaev, D. Garcia and J. Guasch and J. Sola, *Phys. Rev. D* 65, 031701 (2002), *JHEP* 06, 059 (2002).
- [10] S. Moretti and D.P. Roy, in Ref. [2].
- [11] T. Plehn, *Phys. Rev. D* 67, 014018 (2003).
- [12] E. Boos and T. Plehn, hep-ph/0304034.
- [13] R.V. Harlander and W.B. Kilgore, hep-ph/0304035.
- [14] D. Cavalli et al., in hep-ph/0203056.
- [15] D.J. Miller, S. Moretti, D.P. Roy and W.J. Stirling, in Ref. [2].
- [16] M. Spira, *Fortsch. Phys.* 46, 203 (1998).
- [17] See, e.g.: M. Antonelli and S. Moretti, hep-ph/0106332 (and references therein).
- [18] See, e.g.: LEP HIGGS Working Group web page, <http://www.cern.ch/LEPHIGGS/>.
- [19] A. Brignole, J. Ellis, G. Ridol and F. Zwimer, *Phys. Lett. B* 271, 123 (1991); A. Brignole, *Phys. Lett. B* 277, 313 (1992); M. A. Diaz and H.E. Haber, *Phys. Rev. D* 45, 4246 (1992).
- [20] M. Carena, J.S. Conway, H.E. Haber and J.D. Hobbs (conveners), proceedings of the Tevatron Run II SUSY/Higgs' Workshop, Fermilab, Batavia, Illinois, USA, February–November 1998, hep-ph/0010338; M. Guchait and S. Moretti, *JHEP* 01, 001 (2002).
- [21] S. Moretti and W.J. Stirling, *Phys. Lett. B* 347, 291 (1995), Erratum, *ibidem* B 366, 451 (1996); A. Djouadi, J. Kalinowski and P.M. Zerwas, *Z. Phys. C* 70, 435 (1996); E. Ma, D.P. Roy and J. Wudka, *Phys. Rev. Lett.* 80, 1162 (1998).
- [22] H. Murayama, I. Watanabe and K. Hagiwara, KEK Report 91{11, January 1992.
- [23] T. Stelzer and W.F. Long, *Comput. Phys. Commun.* 81, 357 (1994).
- [24] A. Djouadi, J. Kalinowski and M. Spira, *Comp. Phys. Commun.* 108, 56 (1998).

- [25] F. Boudjema and A. Semenov, *Phys. Rev. D* 66 (2002) 095007 [[arXiv:hep-ph/0201219](#)].
- [26] J.F. Gunion and H.E. Haber, *Phys. Rev. D* 67 (2003) 075019 [[arXiv:hep-ph/0207010](#)].
- [27] A. Arhrib and G. Moultaka, *Nucl. Phys. B* 558, 3 (1999).
- [28] G.P. Lepage, *Jour. Comp. Phys.* 27, 192 (1978).
- [29] H. Kharraziha and S.M. Moresi, *Comp. Phys. Comm.* 127, 242 (2000), Erratum, *ibidem* B 134, 136 (2001).
- [30] R. Kleiss, W.J. Stirling and S.D. Ellis, *Comput. Phys. Commun.* 40, 359 (1986).
- [31] See <http://durpdg.dur.ac.uk/hepdata/pdf.html> for an up-to-date compilation of PDFs.
- [32] F. Gianotti, M.L. Mangano, T. Virdee (conveners), [hep-ph/0204087](#).
- [33] ATLAS Inner Detector, Technical Design Report, Volume I, 10 April 1997.
- [34] T. Sjöstrand, P. Eden, C. Friberg, L. Lönnblad, G. Miu, S. Mrenna and E. Norrbin, *Comput. Phys. Commun.* 135, 238 (2001).

Diagrams by MadGraph

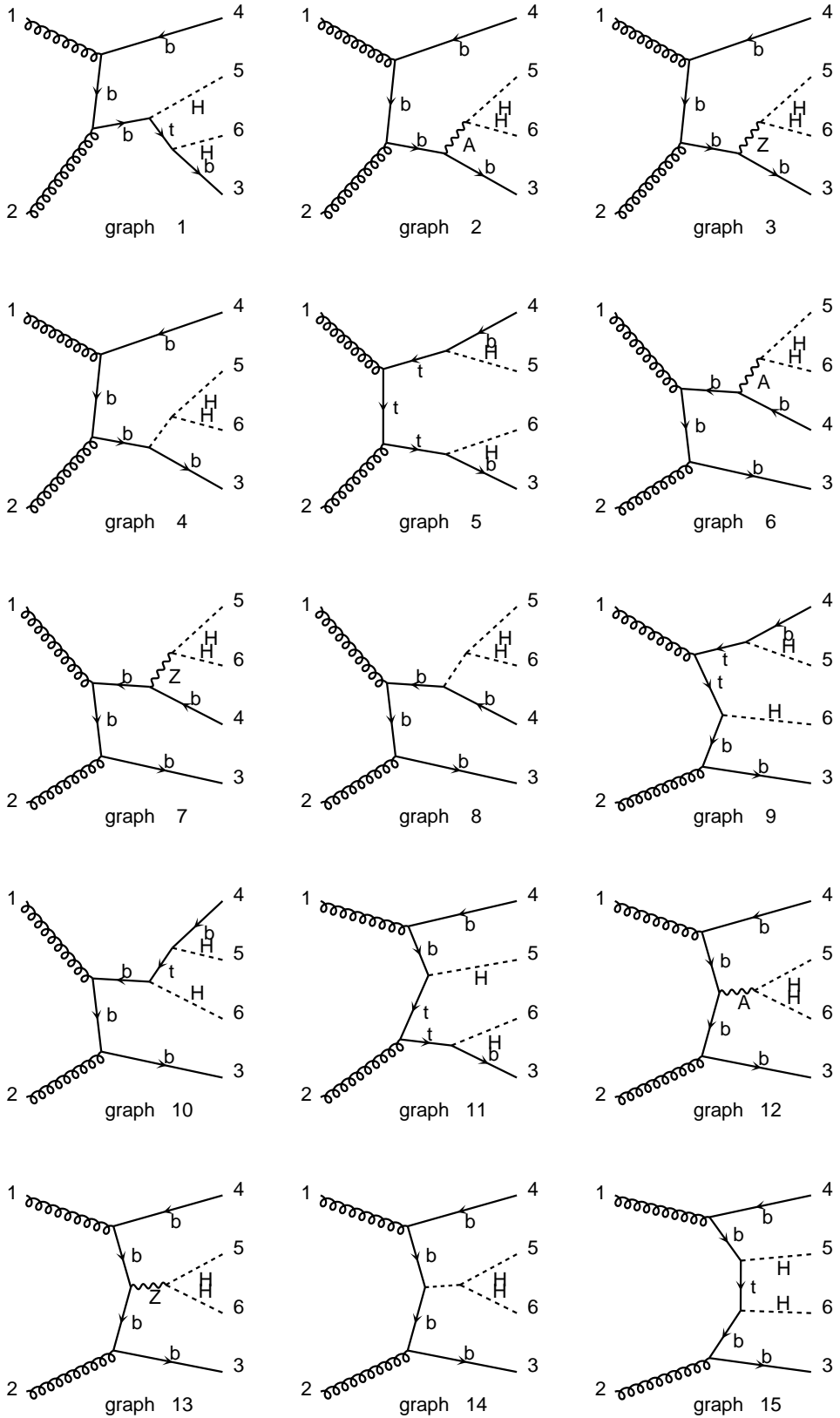


Figure 1: Feynman diagrams in the unitary gauge for process (1).

Diagrams by MadGraph

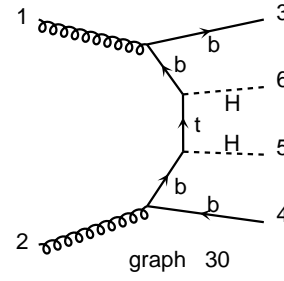
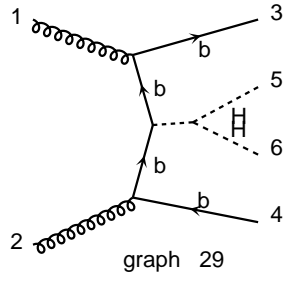
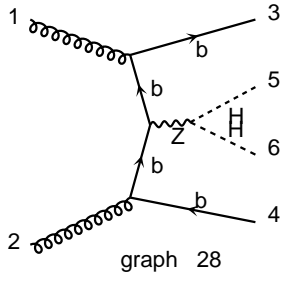
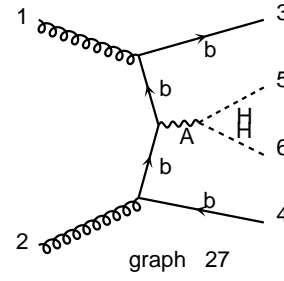
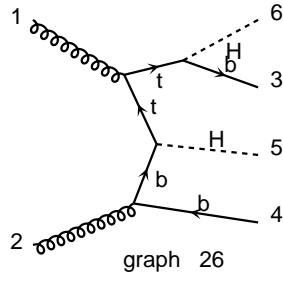
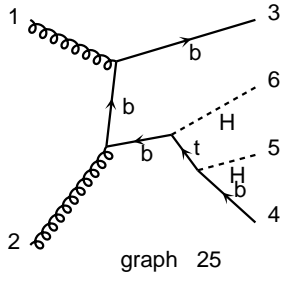
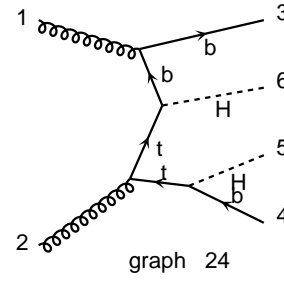
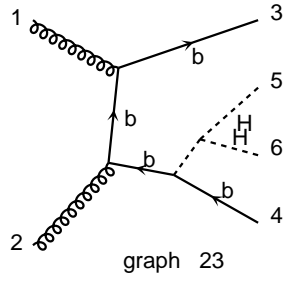
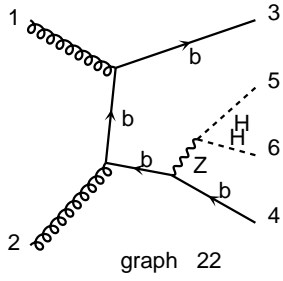
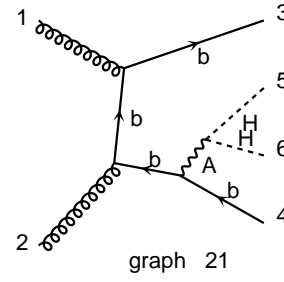
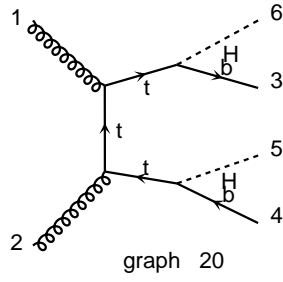
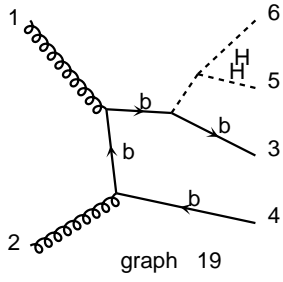
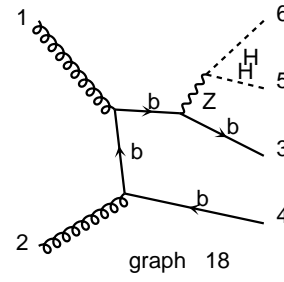
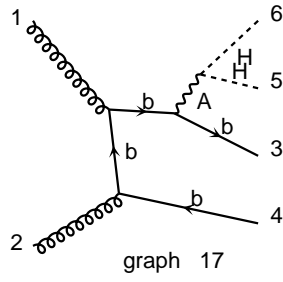
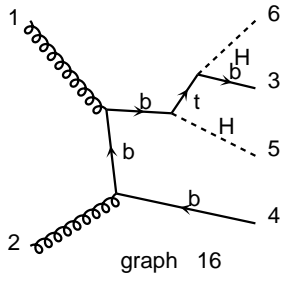


Figure 1: continued

Diagrams by MadGraph

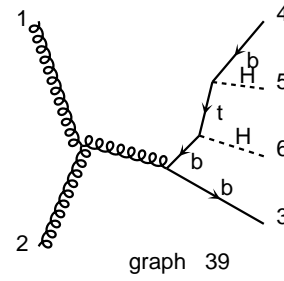
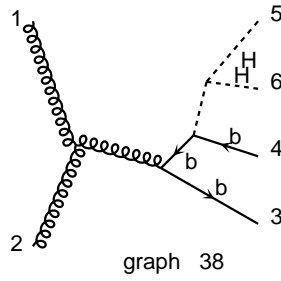
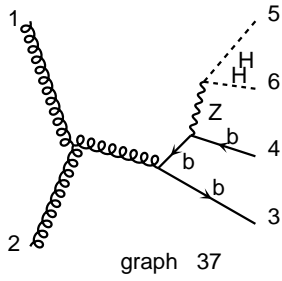
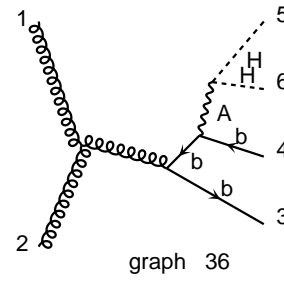
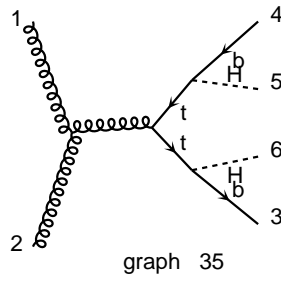
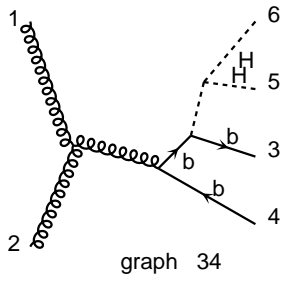
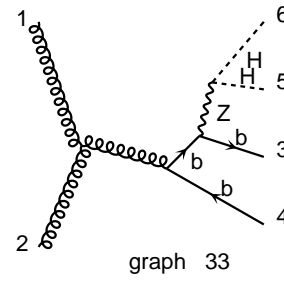
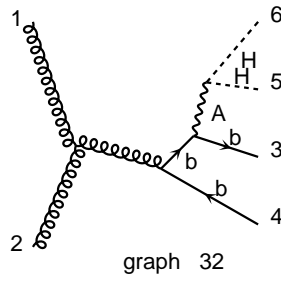
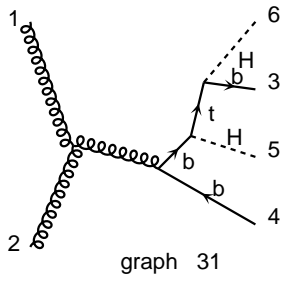


Figure 1: continued

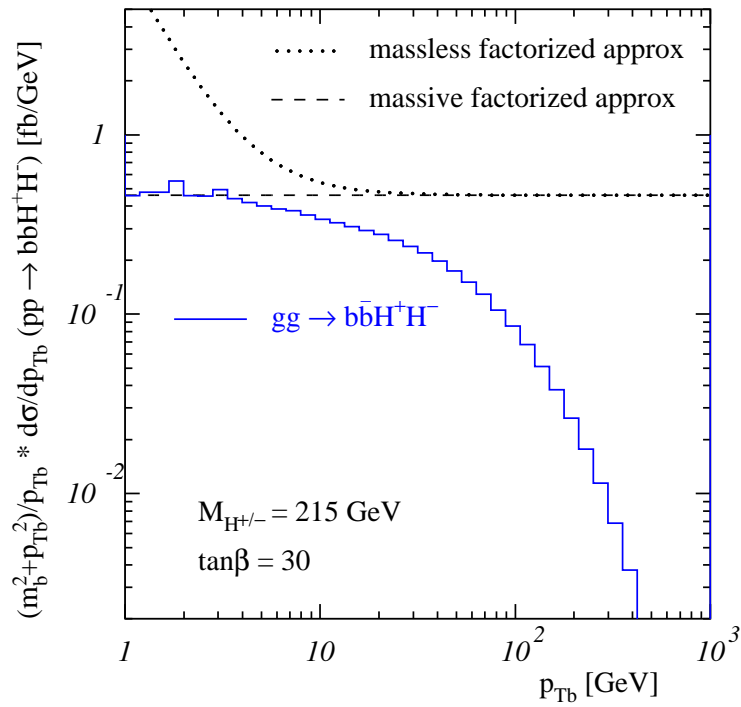


Figure 2: Transverse momentum distribution (multiplied by  $((p_b^T)^2 + m_b^2)/p_b^T$ ) of b-quarks ( $m_b = 4.25 \text{ GeV}$ ) in  $gg \rightarrow bbH^+H^-$  compared to factorised expectations for massless and massive partons.

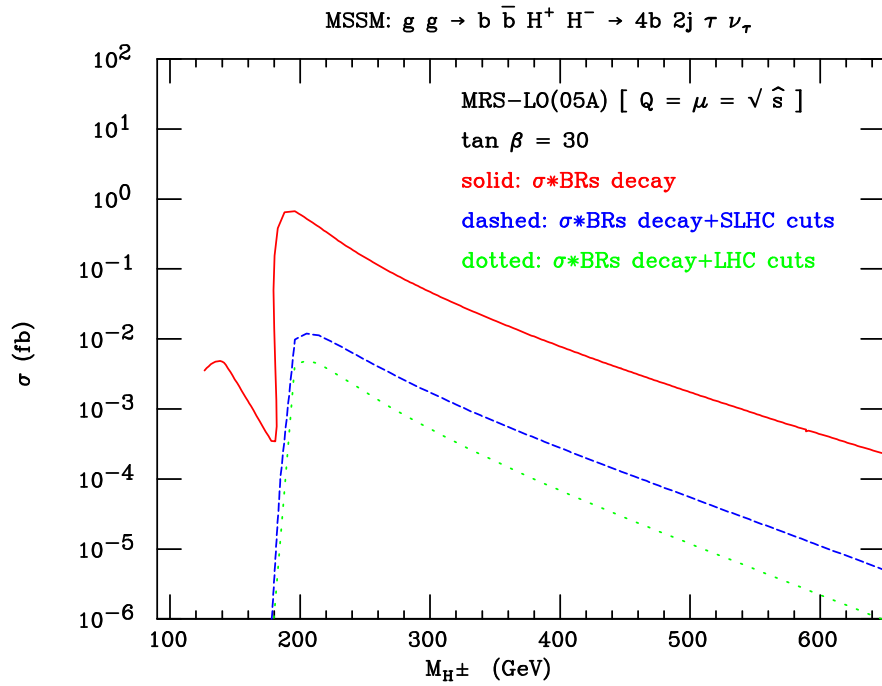


Figure 3: Total cross sections as a function of  $M_{H^\pm}$  for process (1) yielding the signature (5), including all decay BRs and with finite width effects, before (solid) and after the kinematic cuts in (6)–(10), assuming LHC (dotted) and SLHC (dashed) detectors. For reference, the value  $\tan \beta = 30$  is adopted. The MSSM described in the text is here assumed.

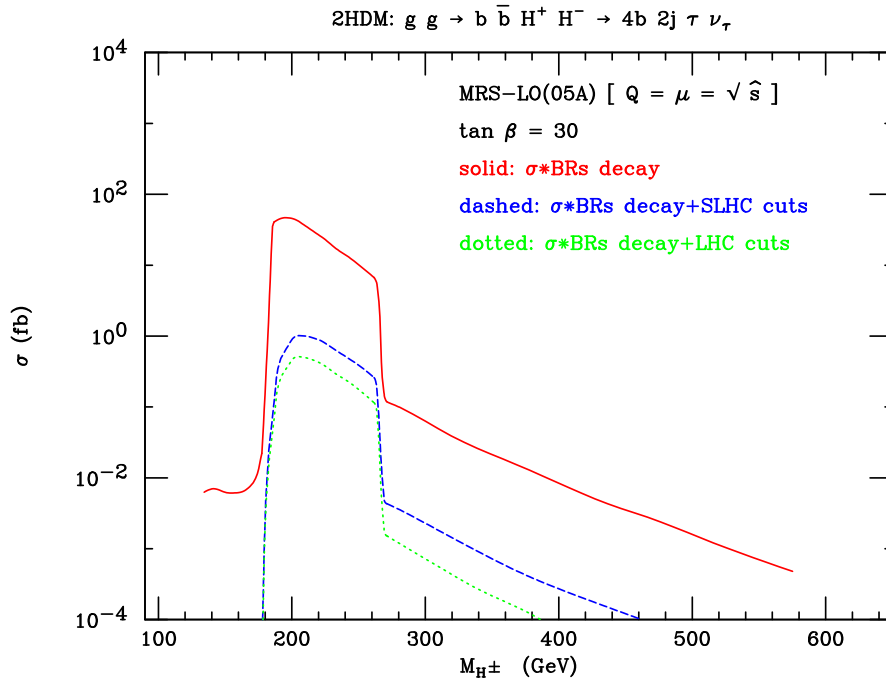


Figure 4: Total cross sections as a function of  $M_{H^\pm}$  for process (1) yielding the signature (5), including all decay BRs and with finite width effects, before (solid) and after the kinematic cuts in (6)–(10), assuming LHC (dotted) and SLHC (dashed) detectors. For reference, the value  $\tan \beta = 30$  is adopted. The 2HDM described in the text is here assumed.

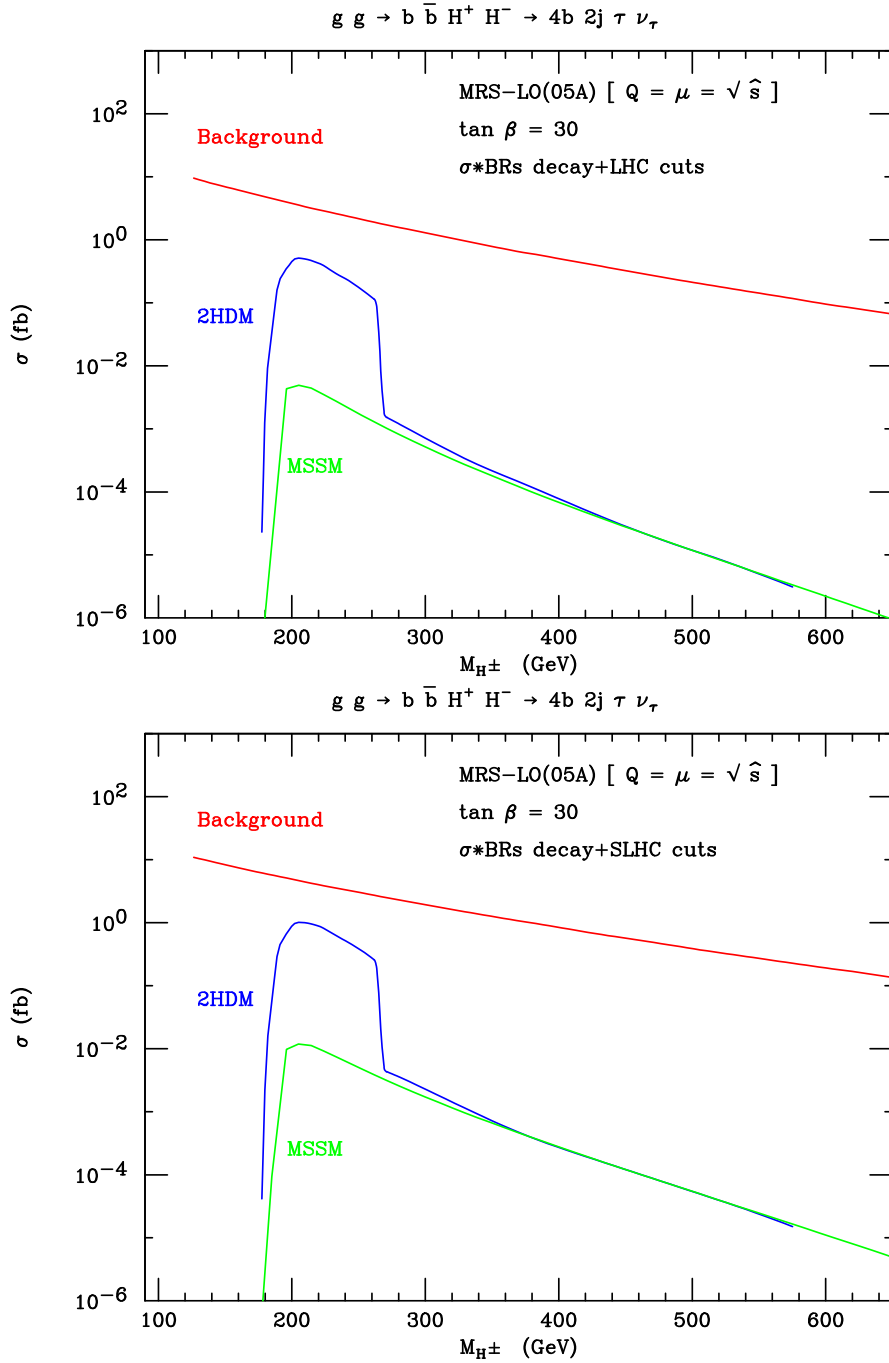


Figure 5: Total cross sections as a function of  $M_{H^\pm}$  for processes (1) (with finite width effects) and (2) yielding the signature (5), including all decay BRs and after the kinematic cuts in (6)-(10), assuming LHC (top) and SLHC (bottom) detectors. For reference, the value  $\tan \beta = 30$  is adopted. The MSSM and the 2HDM described in the text are here compared. (Notice that the background retains a dependence upon  $M_{H^\pm}$  because of the optimisation of the cuts in (7) and (10).)

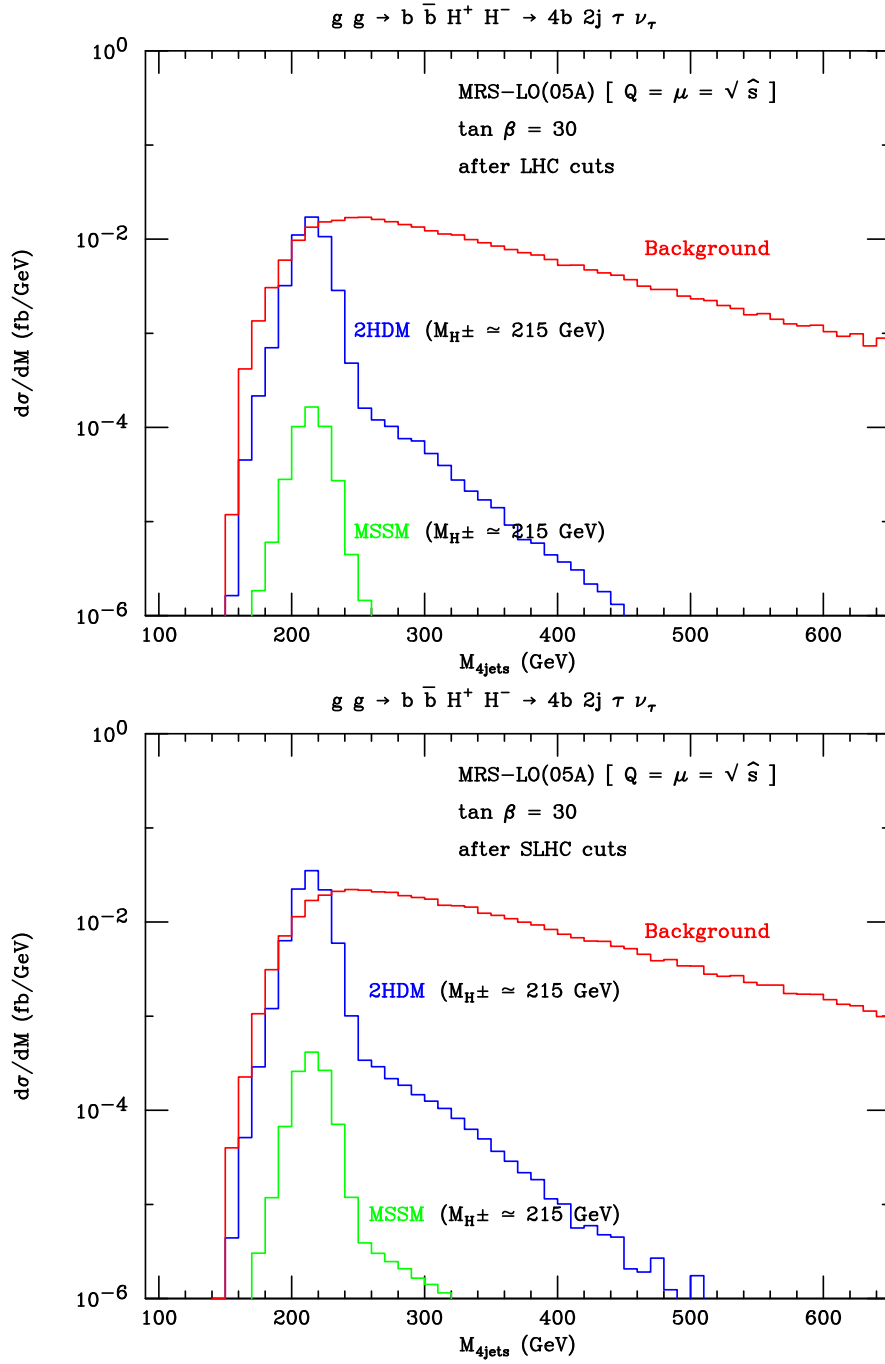


Figure 6: Differential distribution in the invariant mass of the ‘four-jet system’ defined in the text for processes (1) (with finite width effects) and (2) yielding the signature (5), including all decay BRs and after the kinematic cuts in (6)–(10), assuming LHC (top) and SLHC (bottom) detectors. For reference, the values  $M_{H^\pm} = 215$  GeV and  $\tan \beta = 30$  are adopted. The MSSM and the 2HDM described in the text are here compared.

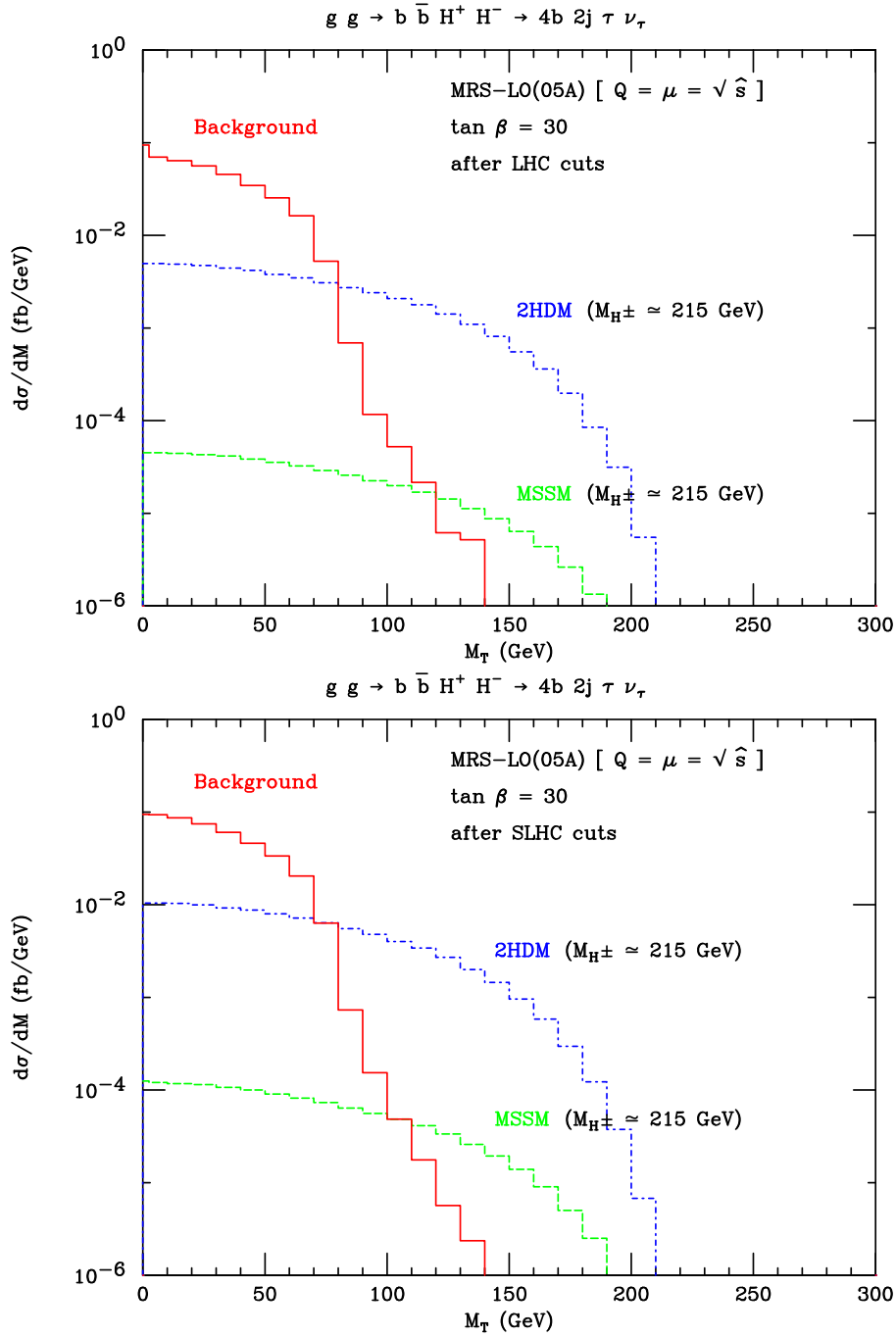


Figure 7: Differential distribution in transverse mass of the ‘tau-neutrino’ system defined in the text for processes (1) (with finite width effects) and (2) yielding the signature (5), including all decay BRs and after the kinematic cuts in (6)–(10), assuming LHC (top) and SLHC (bottom) detectors. For reference, the values  $M_{H^\pm} = 215$  GeV and  $\tan \beta = 30$  are adopted. The MSSM and the 2HDM described in the text are here compared.

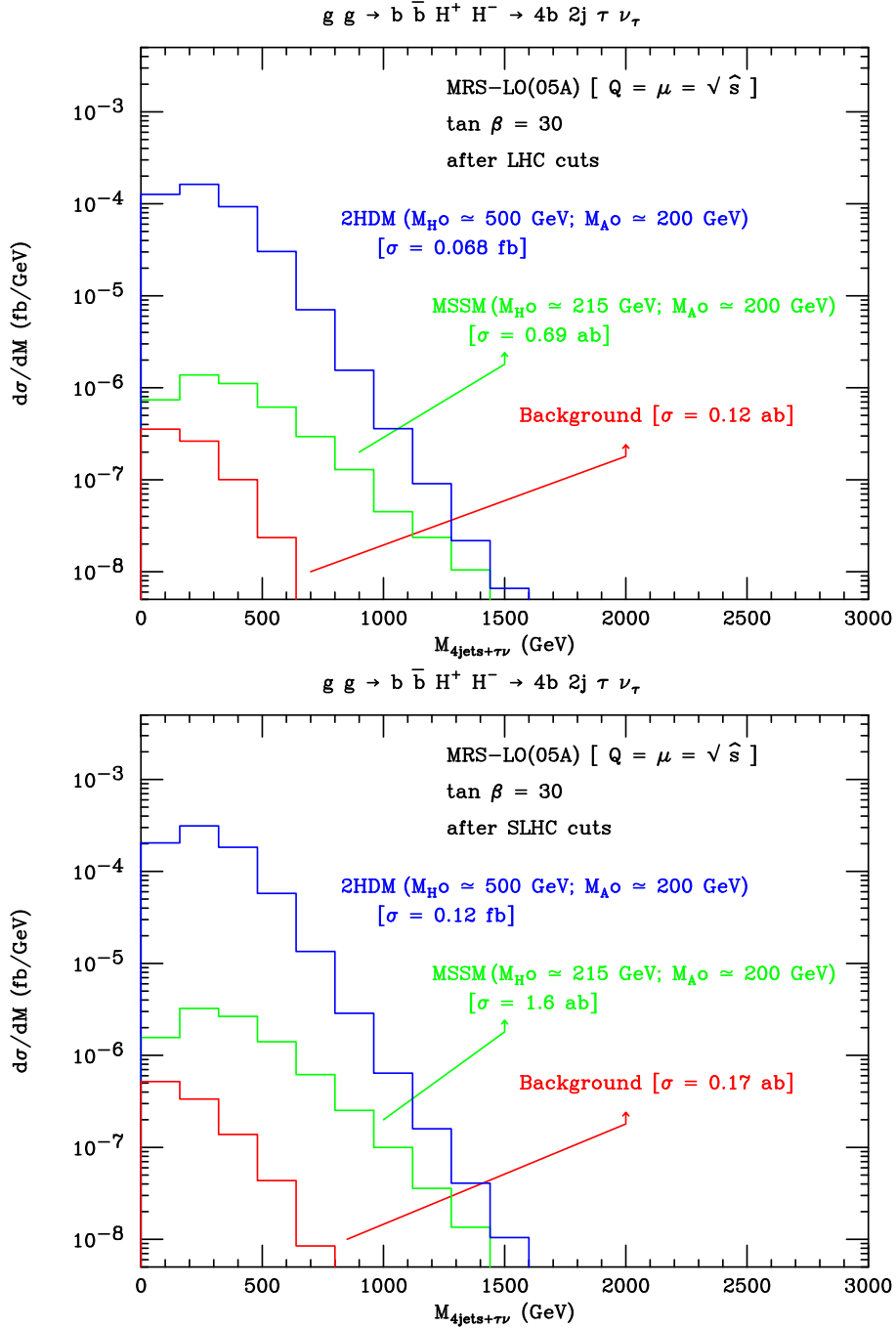


Figure 8: Differential distribution in transverse mass of the ‘four-jets plus tau-neutrino’ system defined in the text for processes (1) (with finite width effects) and (2) yielding the signature (5), including all decay BRs and after the kinematic cuts in (6) (11) and (13), assuming LHC (top) and SLHC (bottom) detectors. For reference, the values  $M_{H^0} = 215$  GeV and  $\tan \beta = 30$  are adopted. The MSSM and the 2HDM described in the text are here compared.

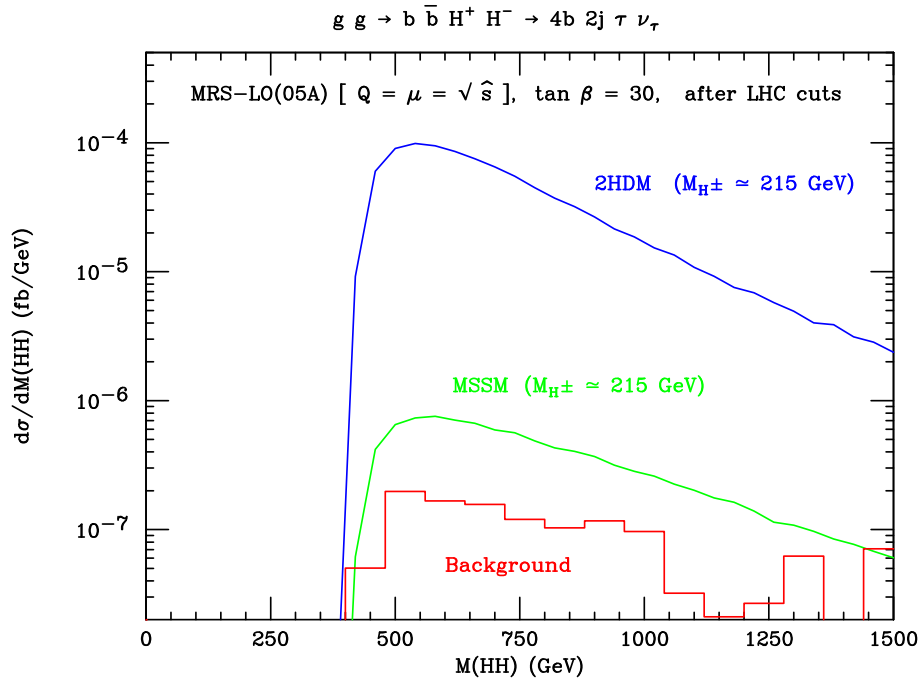


Figure 9: Differential distribution in invariant mass of the ‘four-jets plus tau-neutrino’ system with the longitudinal neutrino momentum reconstructed from the mass-constraint as explained in the text for processes (1) (with finite width effects) and (2) yielding the signature (5), including all decay BRs and after the kinematic cuts in (6) (11) and (13), assuming LHC detectors. For reference, the values  $M_{H^\pm} = 215 \text{ GeV}$  and  $\tan \beta = 30$  are adopted. The MSSM and the 2HDM described in the text are here compared.

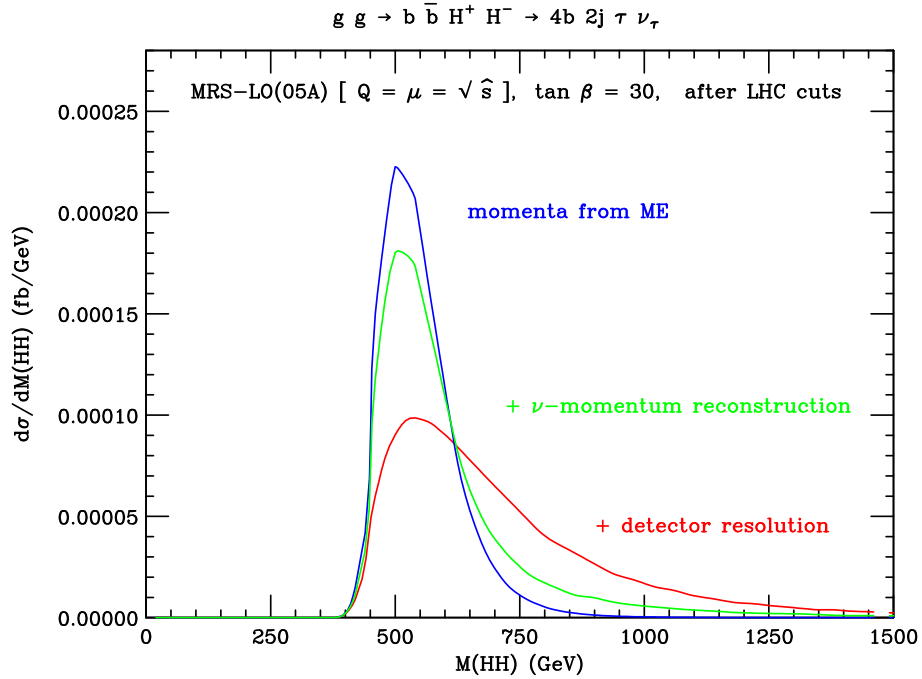


Figure 10: Illustration of the smearing of the signal in the 2HDM due to finite detector resolution and reconstruction of the longitudinal neutrino momentum from the mass-constraint as explained in the text for processes (1) yielding the signature (5), including all decay BRs and after the kinematic cuts in (6)–(11) and (13), assuming LHC detectors. For reference, the values  $M_H = 215$  GeV and  $\tan \beta = 30$  are adopted.